Enhancement of Sea Ice Drift due to the Dynamical Interaction between Sea Ice and a Coastal Ocean

YOSHIHIRO NAKAYAMA*

Graduate School of Environmental Science, Hokkaido University, Sapporo, Japan

KAY I. OHSHIMA AND YASUSHI FUKAMACHI

Institute of Low Temperature Science, Hokkaido University, Sapporo, Japan

(Manuscript received 17 January 2011, in final form 10 August 2011)

ABSTRACT

Wind factor, the ratio of sea ice drift speed to surface wind speed, is a key factor for the dynamics of sea ice and is generally about 2%. In some coastal oceans, however, the wind factor tends to be larger near the coast. This study proposes the enhancement mechanism of the sea ice drift caused by the dynamical coupling between sea ice and a coastal ocean. In a coastal ocean covered with sea ice, wind-forced sea ice drift excites coastal trapped waves (shelf waves) and generates fluctuating ocean current. This ocean current can enhance sea ice drift when the current direction is the same as that of the wind-driven drift. The authors consider a simplified setting where spatially uniform oscillating wind drifts sea ice parallel to the coast. When a barotropic long shelf wave is assumed for the ocean response, sea ice drifts driven by wind and ocean are obtained analytically. The ratio of ocean-driven to wind-driven sea ice drifts is used for the evaluation of the oceanic contribution to the enhancement of sea ice drift. The enhancement is mostly determined by the characteristics of the shelf waves, and sea ice drift is significantly enhanced close to the coast with lower-frequency wind forcing. Comparison with the observation off the Sakhalin coast shows that the degree of enhancement of sea ice drift and its characteristic such that larger enhancement occurs near the coast are mostly consistent with our theoretical solution, suggesting that this mechanism is present in the real ocean.

1. Introduction

Sea ice drift is determined as a result of wind forcing and ice–ocean interaction. Studies on sea ice drift can be traced back to Nansen (1902), who found that sea ice drifts with a speed of about 2% of the surface wind and about 25° to the right of the wind in the Northern Hemisphere.

Recently, sea ice drift has been studied using drifting-buoy and satellite-microwave data in the entire polar sea ice regions (e.g., Thorndike and Colony 1982; Emery et al. 1997; Heil and Allison 1999; Kimura and Wakatsuchi 2000; Kimura 2004). These studies showed that the correlation between wind and sea ice drift tends to be lower in the coastal ocean where sea ice concentration is high. This is caused by the internal stress of sea ice, which can be comparable to the wind stress in the force balance in the extreme case.

Even in a coastal ocean where sea ice concentration is high, the free drift of sea ice, which is not affected by the internal stress, roughly holds in a nonconvergent regime of sea ice drift. Such situation occasionally occurs in the Sakhalin coast in the Sea of Okhotsk and the northern Alaskan coast in the Chukchi Sea. In these regions, correlation between wind and sea ice drift is as high as that away from the coast. It is also noticeable that the wind factor calculated from satellite-microwave data tends to be larger in these regions (Kimura and Wakatsuchi 2000). To be strict, wind factor is defined as the ratio of wind-driven component of sea ice drift to wind speed. However, wind factor is sometimes calculated only from the time series of wind and sea ice drift, neglecting the temporal variation of ocean current underneath the sea ice, because of the lack of ocean current observation. In these cases, the wind factor consequently contains the

* Current affiliation: Alfred Wegener Institute, Bremerhaven, Germany.

Corresponding author address: Yoshihiro Nakayama, Alfred Wegener Institute, Bussestrasse 24 D-27570 Bremerhaven, Germany. E-mail: yoshihiro.nakayama@awi.de.

DOI: 10.1175/JPO-D-11-018.1

effect of temporally varying ocean current. Therefore, the temporal variation of ocean current possibly increases or decreases the wind factor calculated from the time series of wind and sea ice drift.

In a coastal ocean, when sea ice drifts under wind forcing, the movement of sea ice exerts water stress to the ocean, which excites coastal trapped waves (CTWs). The fluctuating ocean current by the CTWs would also drift sea ice in turn. If the sea ice drift driven by wind and ocean current are in the same direction, the sea ice drift is enhanced. Therefore, the larger value of wind factor calculated from satellite-microwave data in a nonconvergent regime of a coastal ocean can be explained by the following coupling mechanism: First, sea ice drifts under wind forcing. Then, the movement of sea ice exerts water stress on the ocean, which excites CTWs and generates fluctuating ocean current. This ocean current enhances the sea ice drift.

Previous direct observations in coastal oceans also showed that sea ice drift is largely influenced by the ocean current and thus the coastal topography (e.g., Pease and Salo 1987; Greenan and Prinsenberg 1998; Häkkinen and Cavalieri 2005; Rabinovich et al. 2007). Fissel and Tang (1991) found that, in the Canadian east coast in the Labrador Sea, the wind factor becomes large under strong wind, and they suggested that it is caused by the wind-driven coastal ocean current. From a coupled ice–ocean model, Overland and Pease (1988) showed that sea ice drift in the coastal ocean is strongly affected by the wind-driven ocean current. These previous studies also suggest that sea ice motion in a coastal ocean is determined as a result of dynamical interaction among wind, a coastal ocean, and sea ice.

The objective of this study is to examine the coupling mechanism between sea ice and a coastal ocean that enhances sea ice drift as described above. We consider this interaction in an idealized setting. We also apply our theory to the real ocean to examine its validity. We use the ratio of the wind factor that contains the effect of ocean current (apparent wind factor) to the exact wind factor that does not contain the effect of ocean current to evaluate the contribution of fluctuating ocean current to sea ice drift in an analytical solution and to compare with the observation.

2. Dynamical interaction between sea ice and a coastal ocean

a. Momentum equation of sea ice in steady state

We consider the case where sea ice drifts under wind forcing. The time scale of sea ice drift considered in this study is longer than a day, which is much longer than the response time of sea ice drift to wind, according to Zubov (1945) and Leppäranta (2005). Thus, in the equation of motion for sea ice, the time derivative term can be neglected. Further we assume that the free drift of sea ice roughly holds and the internal stress term can be neglected. Under these conditions, the motion of sea ice is determined by the balance of wind and water stresses and the Coriolis force, represented by

$$\boldsymbol{\tau}_a + \boldsymbol{\tau}_w + \mathbf{R}(\pi/2)\rho_{\text{ice}} hf(\mathbf{u}_w - \mathbf{u}_{\text{ice}}) = 0, \qquad (1)$$

where wind and water stresses are given with the quadratic form for simplicity as

$$\boldsymbol{\tau}_a = \rho_a C_a |\mathbf{U}_a| \mathbf{U}_a \quad \text{and} \qquad (2)$$

$$\boldsymbol{\tau}_w = \mathbf{R}(\theta_w)\rho_w C_w |\mathbf{u}_w - \mathbf{u}_{\text{ice}}|(\mathbf{u}_w - \mathbf{u}_{\text{ice}}) \qquad (3)$$

and rotation matrix $\mathbf{R}(\theta_0)$ is

$$\mathbf{R}(\theta_0) = \begin{pmatrix} \cos\theta_0 & -\sin\theta_0 \\ \sin\theta_0 & \cos\theta_0 \end{pmatrix}, \qquad (4)$$

where θ_0 is an arbitrary angle.

In these equations, $\mathbf{u}_{\text{ice}}$, $\mathbf{U}_a$, and $\mathbf{u}_w$ are sea ice, surface wind, and ocean current velocities; ρ_a, ρ_w, and ρ_{ice} are densities of air, water, and sea ice; C_a and C_w are air–ice and ice–water drag coefficients; h is sea ice thickness; and f is the Coriolis parameter. The angle θ_w is the turning angle by which the direction of $\boldsymbol{\tau}_w$ is rotated from the direction of $(\mathbf{u}_w - \mathbf{u}_{\text{ice}})$ because of the Ekman veering.

Generally, sea ice velocity of free drift can be expressed as

$$\mathbf{u}_{\text{ice}} = \alpha \mathbf{R}(-\theta)\mathbf{U}_a + \mathbf{u}_w, \qquad (5)$$

where α is wind factor and θ is the angle between $(\mathbf{u}_{\text{ice}} - \mathbf{u}_w)$ and $\mathbf{U}_a$. Substitution of Eqs. (2), (3), and (5) into Eq. (1) yields the following equations (Leppäranta 1998):

$$\alpha^4 + 2\sin\theta_w \text{RoNa}\alpha^3 + \text{Ro}^2\text{Na}^2\alpha^2 - \text{Na}^4 = 0 \quad \text{and} \qquad (6)$$

$$\theta = \arctan\left(\tan\theta_w + \frac{\text{RoNa}}{\alpha\cos\theta_w}\right). \qquad (7)$$

The Nansen number Na is defined as

$$\text{Na} = \sqrt{\frac{\rho_a C_a}{\rho_w C_w}}, \qquad (8)$$

which is equivalent to the wind factor for the case where the Coriolis force is negligible and sea ice drifts with the

exact balance between wind and water stresses. The ice Rossby number Ro is defined as

$$\mathrm{Ro} = \frac{\rho_{\mathrm{ice}} f h}{\rho_w C_w \mathrm{Na} |\mathbf{U}_a|}, \tag{9}$$

where larger ice Rossby number means stronger effect of the Coriolis force on sea ice drift. From Eq. (6), sea ice roughly drifts with $\alpha = \mathrm{Na}$ when Ro is small (when wind speed is large and/or sea ice is thin).

McPhee (1979) showed that the quadratic drag relation is somewhat different from the result of either boundary layer theory or observation, and the drag should be approximately proportional to $(\mathbf{u}_w - \mathbf{u}_{\mathrm{ice}})^{1.7}$. Using a more realistic Rossby similarity scale method of the boundary layer theory, C_w decreases with increase of wind speed (McPhee 1981, 2008) and wind factor (Nansen Number) becomes the function of wind speed. Thus, when wind speed increases from 5 to 15 m s^{-1}, for example, wind factor (Nansen number) increases by about 10%. Therefore, in reality, wind factor would vary with wind speed even in the absence of fluctuating ocean currents. However, because we would like to evaluate the coupling mechanism between sea ice and a coastal ocean that enhances sea ice drift in a simplified setting, the quadratic drag relation is assumed in this study.

In the case where free drift of sea ice roughly holds, deformation rate of sea ice remains small and sea ice flow can be assumed as the Newtonian fluid. With this assumption, the Ekman transport can be calculated by integrating momentum equation from the surface to a level of zero stress and the total mass transport of the ice and ocean occurs in the direction 90° to the right of the wind stress in the Northern Hemisphere. If the Ekman transport has the component perpendicular to the coast, it results in a compensating flux in the layer underneath, generating CTWs through stretching or shrinking of water column (Gill and Schumann 1974).

b. *Shelf waves excited by wind stress on sea ice*

In this subsection, we take an analytical approach on oceanic motion excited by wind stress on sea ice in an idealized setting in a coastal ocean. A right-handed coordinate system is chosen such that the positive y axis points seaward from the coast and the x axis lies along the coastline at $y = 0$ (Fig. 1). The depth of ocean is given as a function of distance from the coast. We assume that ocean surface is completely covered with sea ice and wind stress uniformly drifts sea ice. From Eq. (5), wind drifts sea ice with a speed of $\alpha|\mathbf{U}_a|$ in the direction θ from the wind. Because the magnitude of the Coriolis force changes with wind speed and ice thickness, the values of α and θ are functions of Ro and Na [Eqs. (6) and (7)]. To model the dynamical interaction between sea ice and a coastal ocean in a simplified setting, however, we assume that α and θ are constant and consider the case where spatially uniform wind oscillating with a specific period drifts sea ice parallel to the coast. We assume Ro is small and thus $\alpha = \mathrm{Na}$. When $\mathrm{Ro} < 0.2$, this approximation is valid with the associated error being less than 10% for the value of α (Leppäranta 2005). We set $\theta = 25°$, following Leppäranta (2005), which is a typical value from the previous observations. Here, the spatially uniform wind oscillating with a specific period that drifts sea ice parallel to the coast is represented by

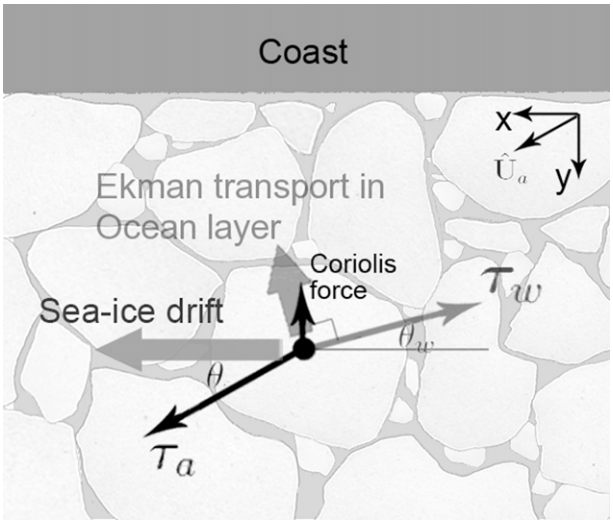

FIG. 1. A schematic diagram showing the force balance of sea ice drift in the Northern Hemisphere. The vectors $\boldsymbol{\tau}_a$ and $\boldsymbol{\tau}_w$ are wind and water stresses. The Coriolis force vector and the Ekman transport in the ocean layer are indicated. Here, θ is the angle between $(\mathbf{u}_{\mathrm{ice}} - \mathbf{u}_w)$ and $\mathbf{U}_a$ and θ_w is the turning angle by which the direction of τ_w is rotated from the direction of $(\mathbf{u}_w - \mathbf{u}_{\mathrm{ice}})$ because of the Ekman veering, where $\mathbf{u}_{\mathrm{ice}}$, $\mathbf{U}_a$, and $\mathbf{u}_w$ are sea ice, surface wind, and ocean current velocities. The arrow with the symbol $\hat{\mathbf{U}}_a$ indicates the direction of the oscillating wind vector. The internal stress of sea ice is not considered, and the mean ocean current $\mathbf{u}_w$ is assumed to be zero here.

$$\mathbf{U}_a = \begin{cases} 0, & y < -(1/\tan\theta)x \\ \hat{\mathbf{U}}_a \dfrac{(|\sin\omega t|)^{1.5}}{\sin\omega t}, & y \geq -(1/\tan\theta)x. \end{cases} \tag{10}$$

This is because in general the scale of atmospheric disturbance is sufficiently larger than that of shelf in the ocean. With this wind forcing [Eq. (10)], wind stress is calculated as $\boldsymbol{\tau}_a = \rho_a C_a |\hat{\mathbf{U}}_a| \hat{\mathbf{U}}_a \sin\omega t$ and we can easily apply the solution of CTWs (Gill and Schumann 1974) in the following. The direction of wind vector $\hat{\mathbf{U}}_a$ is θ from the coast (Fig. 1), which drifts sea ice parallel to the coast. Because horizontally uniform wind stress at the surface generates the uniform Ekman transport perpendicular

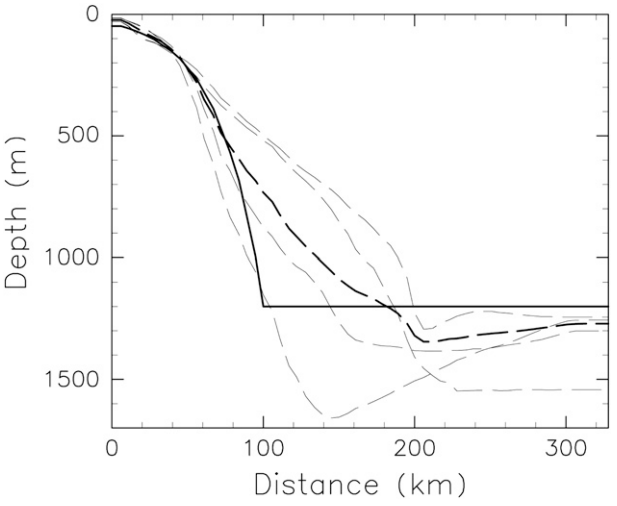

FIG. 2. Depth profiles off the Sakhalin coast (dashed line) and a fitted exponential depth profile (solid line). Four thin dashed lines show the averaged depth profiles for every 1° over 49°–53°N. The thick dashed line shows the averaged depth profile over 49°–53°N. The exponential depth profile fitted to the real depth profile has the constants $\lambda = 1.7 \times 10^{-2}$ km^{-1}, $L = 100$ km, and $H_0 = 40$ m in Eq. (15).

to the wind stress, the Ekman transport is blocked at the coast in $x \geq 0$ and induces CTWs.

The motion of ocean underneath sea ice is assumed to be barotropic CTWs excited by the across-shore component of the Ekman transport. We apply the model developed by Gill and Schumann (1974) to solve for the barotropic CTWs. [In the following, the term ''shelf wave'' is used for barotropic CTWs following Gill and Schumann (1974)]. The Ekman transport in the ocean layer is generated in the direction 90° to the right of $\boldsymbol{\tau}_w$ (Fig. 1), and its across-shore component is $|\boldsymbol{\tau}_w|\cos\theta_w/(\rho_w f)$. From the force balance of sea ice in the alongshore direction, $|\boldsymbol{\tau}_w|\cos\theta_w = |\boldsymbol{\tau}_a|\cos\theta$ is obtained (Fig. 1). As described in section 2a, the wind stress generates the Ekman transport in the ice/ocean layer in the direction 90° to the right of the wind stress. The across-shore component of this transport is $|\boldsymbol{\tau}_a|\cos\theta/(\rho_w f)$, which is equivalent to the across-shore transport generated by $\boldsymbol{\tau}_w$ in the ocean layer. This is because sea ice drifts only in the alongshore direction and there is no across-shore component of the Ekman transport in the ice layer. In the equations of motion, $|\boldsymbol{\tau}_a|\cos\theta$ should be represented by the cross product of $\mathbf{i}$ (unit vector along x axis) and $\boldsymbol{\tau}_a$ to take into account for the direction of $\boldsymbol{\tau}_a$. Assuming the rigid-lid and long-wave approximations and neglecting nonlinear terms, the equations of motion and continuity equation are

$$\frac{\partial u_w}{\partial t} - f v_w = -g\frac{\partial \eta}{\partial x} + \frac{\boldsymbol{\tau}_a \cdot \mathbf{i}}{\rho_w H}, \tag{11}$$

$$f u_w = -g\frac{\partial \eta}{\partial y}, \quad \text{and} \tag{12}$$

$$\frac{\partial}{\partial x}(H u_w) + \frac{\partial}{\partial y}(H v_w) = 0. \tag{13}$$

Here, u_w and v_w are alongshore and across-shore components of $\mathbf{u}_w$, and H, η, and g are the depth of ocean, elevation of sea surface, and acceleration due to gravity. The motion of ocean is solved from the vorticity equation by introducing a streamfunction (Gill and Schumann 1974), and the alongshore component of ocean current is calculated as a summation of all modes represented by

$$u_w(x,y,t) = \sum_n \frac{2\rho_a C_a |\hat{\mathbf{U}}_a|^2 b_n c_n \cos\theta}{f H \rho_w \omega} \times \sin\left(\frac{\omega x}{2c_n}\right) \sin\omega\left(t - \frac{x}{2c_n}\right) F_n'(y). \tag{14}$$

Here, $F_n(y)$ is the eigenfunction and b_n and c_n are constants determined from the depth profile. Substitution of Eq. (14) into Eq. (5) yields the total velocity of sea ice.

c. Case with an exponential depth profile

As in Gill and Schumann (1974), we first consider the case with an exponential depth profile represented by

$$H = \begin{cases} H_0 e^{2\lambda y} & (y \leq L) \\ H_0 e^{2\lambda L} & (y > L). \end{cases} \tag{15}$$

The exponential depth profile is convenient because the solution can be obtained analytically. The eigenfunctions $F_n(y)$ are obtained as

$$F_n(y) = A_n e^{\lambda y} \sin\beta_n y, \tag{16}$$

where A_n and β_n are constants determined from the depth profile.

In the following, we set various parameters based on the case off the Sakhalin coast in the Sea of Okhotsk. The exponential depth profile is obtained by fitting to the real shelf topography (Fig. 2). Based on the typical wind forcing off the Sakhalin coast discussed in section 3a, $|\hat{\mathbf{U}}_a| = 7$ m s^{-1} and $\omega = 0.1$ cpd are used. Values of C_a and C_w have been measured in various sea ice–covered oceans (e.g., Smith 1972; Banke et al. 1980; Joffre 1982; McPhee 1982; Pease et al. 1983; Martinson and Wamser 1990; Andreas and Claffey 1995; Fujisaki et al. 2009). The values of measured C_a and C_w vary widely, depending on the sea ice condition such as roughness of sea ice. In this study, we set typical values of $C_a = C_w = 2.0 \times 10^{-3}$. With these values, Na = 0.035.

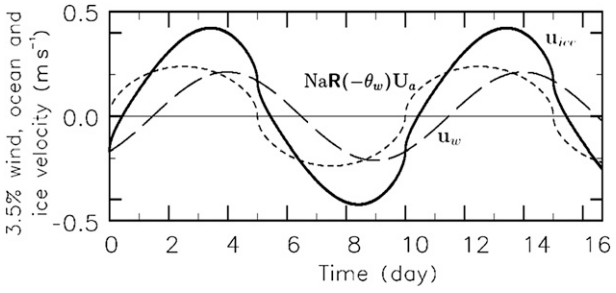

FIG. 3. Time series of wind-driven sea ice velocity $\mathrm{Na}\mathbf{R}(-\theta)\mathbf{U}_a$ (dotted line), ocean current $\mathbf{u}_w$ (dashed line), and total sea ice velocity $\mathbf{u}_{\mathrm{ice}}$ (thick solid line) at $x = 250$ km and $y = 0$ km. In this case, $\mathrm{Na}\mathbf{R}(-\theta)\mathbf{U}_a$ is 3.5% of wind speed.

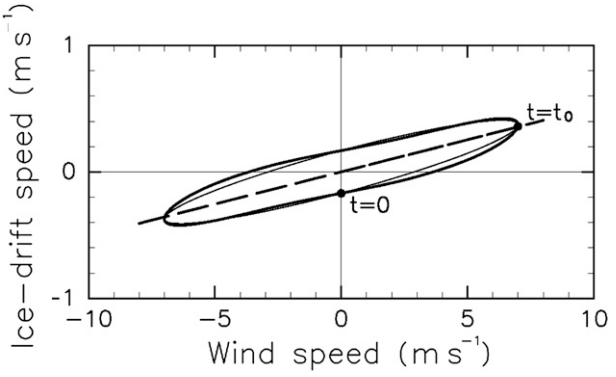

FIG. 4. The trajectory of the wind speed of $X = |\hat{\mathbf{U}}_a|(|\sin\omega t|)^{1.5}/\sin\omega t$ and the sea ice drift of $Y = \mathrm{Na}|\hat{\mathbf{U}}_a|(|\sin\omega t|)^{1.5}/\sin\omega t + u_w$ at $x = 250$ km, $y = 0$ km, which is the same location as in Fig. 3. The thin line indicates the ellipse, which passes through the same points as the trajectory of X and Y when X is 0, the minimum and maximum. The dashed line indicates an approximated linear function of the trajectory of X and Y obtained by a least squares method. The dot with $t = 0$ indicates the time when wind speed is zero, and the dot with $t = t_0$ indicates the time when the wind speed is the maximum.

Time series of wind-driven sea ice velocity $\mathrm{Na}\mathbf{R}(-\theta)\mathbf{U}_a$, ocean current $\mathbf{u}_w$, and total sea ice velocity $\mathbf{u}_{\mathrm{ice}}$ at $x = 250$ km and $y = 0$ km calculated from Eqs. (5) and (14) are shown in Fig. 3. In this case, $\mathbf{u}_{\mathrm{ice}}$ is generally enhanced by $\mathbf{u}_w$ because $\mathrm{Na}\mathbf{R}(-\theta)\mathbf{U}_a$ and $\mathbf{u}_w$ do not have a large phase difference and are in the same direction for most of the time. However, there exists a short period of time when $\mathbf{U}_a$ and $\mathbf{u}_w$ are in the opposite directions and $\mathbf{u}_{\mathrm{ice}}$ is weakened. From Eqs. (10) and (14), the phase difference between $\mathbf{U}_a$ and $\mathbf{u}_w$ is $\omega x/2c_n$, which can take all the values in 0–2π, depending on x. Therefore, depending on x, $\mathbf{u}_{\mathrm{ice}}$ can be enhanced or weakened by $\mathbf{u}_w$ in principle. However, the mode 1, which is the dominant mode in general, has relatively small phase difference within the general alongshore scale of the coast. Consequently, sea ice drift is generally enhanced. In the case off the Sakhalin coast, for example, the antiphase (π) point of the mode 1 occurs at $x = 4400$ km, suggesting that $\mathbf{u}_{\mathrm{ice}}$ is mostly enhanced by $\mathbf{u}_w$. To define the enhancement of sea ice drift due to ocean current precisely, however, we still need to isolate the influence of phase difference in time. One simple way to achieve this is to discuss an averaged value of the enhancement of sea ice drift over some time span.

d. Apparent wind factor

To be strict, wind factor is defined as the ratio of wind-driven component of sea ice drift to wind speed, which is denoted as the exact wind factor in this study. In this study, we consider the case where Ro is small and assume that the exact wind factor equals to the Nansen number. However, wind factor is sometimes obtained only from the time series of sea ice drift and wind due to the lack of ocean current observation. Thorndike and Colony (1982) calculated α and θ using a least squares method by neglecting the time variation of α, θ, and $\mathbf{u}_w$ in Eq. (5) from the time series of sea ice drift and geostrophic wind. The wind factor calculated by this method would be modified by the influence of fluctuating ocean current. Kimura and Wakatsuchi (2000) and Kimura (2004) also calculated the value of wind factor using the same method based on the satellite-microwave and geostrophic wind data. In this study, we define the wind factor obtained by this method as apparent wind factor to be distinguished from the exact wind factor. In the above method, the apparent wind factor is generally calculated from the time series over some time span. Namely, the apparent wind factor obtained in these observations is actually the averaged ratio of sea ice drift driven by both wind and fluctuating ocean current to wind speed.

As pointed out by the theoretical discussion in the previous subsection, the enhancement of sea ice drift due to fluctuating ocean current should also be evaluated over some time span. This concept is similar to that of the apparent wind factor used in the previous observational studies. Therefore, we define the apparent wind factor in the same manner for the analytical solutions. Because the value of turning angle θ is assumed to be constant, we define the apparent wind factor from the time series of wind speed and sea ice speed using a least squares method. When we set X as wind speed in the direction of $\hat{\mathbf{U}}_a$ and Y as sea ice speed along the x-axis direction, $X = |\hat{\mathbf{U}}_a|(|\sin\omega t|)^{1.5}/\sin\omega t$ and $Y = \mathrm{Na}|\hat{\mathbf{U}}_a|(|\sin\omega t|)^{1.5}/\sin\omega t + u_w$. Because X and Y are functions of time, the trajectory of X and Y can be plotted in the x–y plane (Fig. 4). When this trajectory is approximated to a linear function (dashed line in Fig. 4) by using a least squares method, the slope of the linear function represents the averaged ratio of sea ice drift

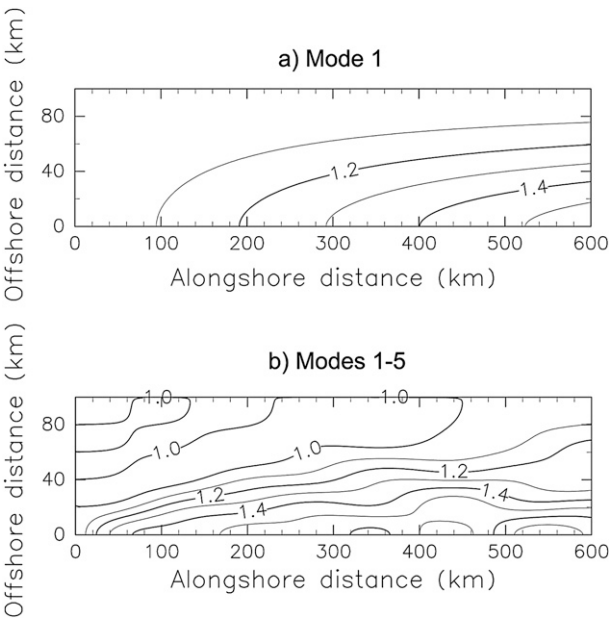

FIG. 5. Spatial distributions of enhancement ratio γ calculated from (a) mode 1 and (b) modes 1–5 for the case with the exponential depth profile fitted to the coast off Sakhalin, for $\hat{\mathbf{U}}_a = 7\ \mathrm{m\ s^{-1}}$ and $\omega = 0.1$ cpd.

to wind speed, which is defined as the apparent wind factor here. Here, we define the time t_0 as the time when the wind speed is the maximum. We assume that the slope of the linear function by a least squares method (dashed line in Fig. 4) can be approximated to the slope of the linear function connecting the origin and the point where $t = t_0$. The reason for this assumption is as follows: The ellipse that passes through the same points as the trajectory of X and Y when X is 0, the minimum and maximum, is plotted (thin line in Fig. 4). It is found that the trajectory shape of X and Y is fairly similar to that of the ellipse. For the case of the ellipse, the slope of the linear function from a least squares method is equivalent to the slope of the linear function connecting the origin and the point where $X^2 + Y^2$ becomes maximum. Furthermore, the time when $X^2 + Y^2$ becomes maximum can be approximated as t_0, because $|\hat{\mathbf{U}}_a| \gg |\mathbf{u}_{\mathrm{ice}}|$. Thus, for the case of ellipse-like trajectory of X and Y, we also assume that the slope of the linear function by using a least squares method can be approximated as the slope of the linear function connecting the origin and the point where $t = t_0$. When two of the slopes are calculated in the range of 0 km $\leq x \leq$ 600 km (range of x in Fig. 5), this assumption is valid with an associated error between these two slopes being less than 5%. Thus, the apparent wind factor is calculated as the ratio of the sea ice to wind speeds at $t = t_0$ in the following.

e. Enhancement of sea ice drift

Here, we define the enhancement ratio of the wind factor γ as the ratio of the apparent to the exact wind factors. Namely, γ is the ratio of sea ice drift driven both by wind and fluctuating ocean current to sea ice drift driven only by wind. When γ is larger than unity, sea ice drift is enhanced by the fluctuating ocean current.

For the case discussed in section 2d, γ is

$$\gamma(x,y) = 1 + \sum_n \frac{\rho_a C_a |\hat{\mathbf{U}}_a| b_n c_n \cos\theta}{fH\mathrm{Na}\rho_w \omega} \sin\left(\frac{\omega x}{c_n}\right) F_n'(y). \tag{17}$$

The enhancement ratio of the wind factor γ is the sum of unity (normalized exact wind factor) and the enhancement of sea ice drift due to the fluctuating ocean current [the second term in Eq. (17)], represented by the summation of the shelf wave modes. Spatial distributions of γ by the mode 1 and the modes 1–5 for the exponential depth profile fitted to the Sakhalin coast described in section 2c are shown in Figs. 5a,b, respectively. The contribution of the modes higher than 5 are negligible, so the summation of the modes 1–5 is considered in this study.

As shown in Eq. (17), γ for each mode has a dependence of sinusoidal function $\sin(\omega x/c_n)$ in the alongshore direction. Because the wavelength of mode 1 is 4200 km, which is much larger than the alongshore scale in general, γ for the mode 1 (Fig. 5a) is greater than unity all along the coast, with values larger in the region closer to the coast and converging to unity offshore. For the case of modes 1–5, the local maximum is found about 550 km downstream, which represents the contribution of the modes 2 and 3 with the wavelengths 1060 and 480 km, respectively. For the both cases, the enhancement by the fluctuating ocean current is only prominent near the coast and nearly absent in the deep ocean offshore.

f. Factors determining the enhancement of sea ice drift

In this subsection, we discuss the factors that determine the enhancement of sea ice drift. Specifically, we examine the dependence of $\gamma - 1$, the enhancement of sea ice drift due to fluctuating ocean current, on the forcings and conditions. As in section 2d, when wind speed is sufficiently large, $\gamma - 1$ approximately equals to the ratio of ocean current to wind-forced sea ice drift at the time t_0. First, we show the determining factors of the ocean current by the shelf waves at the time t_0 and then present the determining factors of the enhancement. From Eq. (14), the ocean current at the time t_0 is represented as

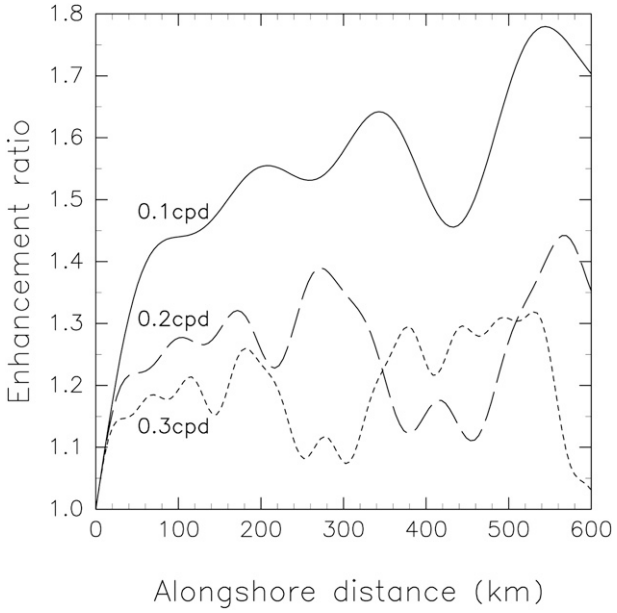

FIG. 6. Dependence of enhancement ratio γ at $y = 0$ km on wind frequency. Results for the cases of the modes 1–5 at 0.1, 0.2, and 0.3 cpd are shown.

$$u_w(x, y, t_0) = \sum_n \frac{\rho_a C_a |\hat{\mathbf{U}}_a|^2 b_n c_n \cos\theta}{fH\rho_w \omega} \sin\left(\frac{\omega x}{c_n}\right) F_n'(y). \tag{18}$$

The ocean current at the time t_0 is proportional to $|\hat{\mathbf{U}}_a|^2$ and C_a. On the other hand, the ocean current does not depend on C_w because the alongshore component of water stress acting on the ocean surface is always balanced with the alongshore component of wind stress. For the case in which $\omega x/c_n \ll 1$, using Taylor expansions, u_w is approximated to

$$u_w(x, y, t_0) = \sum_n \frac{\rho_a C_a |\hat{\mathbf{U}}_a|^2 b_n \cos\theta}{fH\rho_w} x F_n'(y), \tag{19}$$

which does not depend on ω. For the case in which $\omega x/c_n$ is not small, the speed of ocean current generally becomes smaller with higher frequency.

Meanwhile, the wind-forced sea ice drift at the time t_0 is equal to $\mathrm{Na}|\hat{\mathbf{U}}_a|$ and is proportional to $|\hat{\mathbf{U}}_a|$ and $\sqrt{C_a/C_w}$. As a result, the enhancement of sea ice drift $\gamma - 1$, the ratio of the ocean current to the wind-forced sea ice drift, is proportional to $|\hat{\mathbf{U}}_a|$ and $\sqrt{C_a C_w}$. For the case $\omega x/c_n \ll 1$, $\gamma - 1$ is not dependent on ω, whereas, for the case in which $\omega x/c_n$ is not small, the frequency dependence of $\gamma - 1$ is complicated, but $\gamma - 1$ generally becomes smaller with higher frequency (Fig. 6).

g. Solution for the steady forcing

In the discussion above, we have considered the case where sea ice drifts under oscillating wind forcing. Also, under steady wind forcing, sea ice drift may be enhanced in the same manner as a result of the coupling mechanism between sea ice and a coastal ocean. In this subsection, we briefly examine the enhancement of sea ice drift under the same setting as sections 2b and 2c but with steady wind forcing.

The ocean current induced by wind-forced sea ice drift can be solved using an arrested topographic wave model (Csanady 1978). We consider the case where steady wind drifts sea ice parallel to the coast represented by

$$\mathbf{U}_s = \begin{cases} \mathbf{0}, & y < -(1/\tan\theta)x \\ \hat{\mathbf{U}}_s, & y \geq -(1/\tan\theta)x. \end{cases} \tag{20}$$

For the case of steady wind forcing, the equation of motion along the x axis is

$$-fv_w = -g\frac{\partial \eta}{\partial x} + \frac{\boldsymbol{\tau}_a \cdot \mathbf{i}}{\rho_w H} - \frac{ru_w}{H}, \tag{21}$$

where r is the coefficient of the bottom friction. In comparison with the case of oscillating wind [Eq. (11)], the term $\partial u_w/\partial t$ is replaced by ru_w/H. By introducing streamfunction, Eqs. (12) and (21) can be reduced to a heat conduction equation (Csanady 1978), and here we have solved this problem by the analogy to the periodic solution, as in Ohshima (2000). We define γ_s as the ratio of sea ice drift driven by both steady wind and ocean current to sea ice drift driven only by steady wind. Here, the steady wind speed off the coast of Sakhalin is calculated as the average wind speed along the direction that drifts sea ice in the alongshore (north–south) direction, and $|\hat{\mathbf{U}}_s| = 4$ m s^{-1} is used. Based on Chapman et al. (1986), $r = 5.0 \times 10^{-4}$ m s^{-1} is used. The calculated spatial distribution of γ_s is shown in Fig. 7. The result is similar to that of the oscillating case (Fig. 5), including larger enhancement of sea ice drift near the coast. The steady solution of γ_s depends on r, and the enhancement near the coast becomes larger with smaller r, which is determined by the structure of the arrested topographic wave.

3. Application to the real oceans

In this section, we consider the case off the Sakhalin coast in the Sea of Okhotsk to compare a theoretical solution with observational results. Then, we apply our theory to the cases off the Arctic and Antarctic coasts.

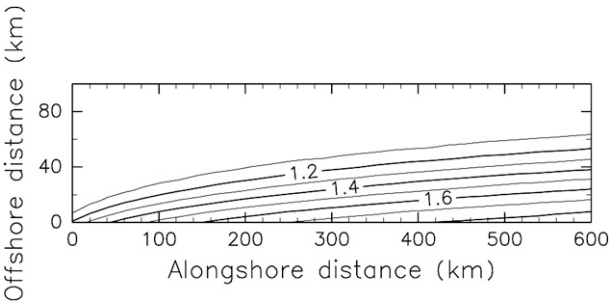

FIG. 7. Spatial distribution of enhancement ratio for the case of steady wind forcing γ_s calculated for the case with the exponential depth profile fitted to the coast off Sakhalin, for $|\hat{\mathbf{U}}_s| = 4$ m s^{-1}.

a. *Application to the coastal region off Sakhalin in the Sea of Okhotsk*

1) RESULT OBTAINED WITH THE REALISTIC BOTTOM TOPOGRAPHY

The exponential depth used in section 2 does not necessarily fit well with the real depth profile. Here, we implement a more realistic topography to allow closer comparison with the observational data obtained in the coastal region off Sakhalin in the Sea of Okhotsk (Fig. 8).

First, we calculate the value of Ro to confirm the applicability of our theory to the Sakhalin coast. The average sea ice thickness off the Sakhalin coast is approximately 1.2 m (Fukamachi et al. 2009), and the typical wind speed is 7 m s^{-1}, as described below. With these parameters, Ro = 0.23, and thus our theory can be applied to the Sakhalin coast.

The depth profile off the Sakhalin coast averaged over 49°–54°N (thick dashed line in Fig. 2) is used for the calculation in this section. Mizuta et al. (2005) showed that CTWs are induced by alongshore wind stress in the Sakhalin coast even in the sea ice season. Under the realistic depth profile and stratification off the Sakhalin coast, located in relatively high latitudes (46°–55°N), the CTWs have nearly barotropic structure (Shevchenko et al. 2004; Mizuta et al. 2005; Ono et al. 2006). In addition, from the dispersion relations, the waves with the period of ~10 days can be treated as long waves. Thus, we assume barotropic long shelf waves as the oceanic response and solve Eqs. (14) and (17) numerically for the realistic topography to obtain the spatial distribution of γ.

Next, we examine the characteristics of the wind forcing based on the European Centre for Medium-Range Weather Forecasts (ECMWF) dataset. The data at the grid point at 52.875°N, 144°E (the location indicated by the asterisk near M1 in Fig. 8) are used. The principal direction of the wind from December 1998 to April 1999 is toward the east-southeast, approximately 60° from the coast. When the Sakhalin coast is assumed to be oriented

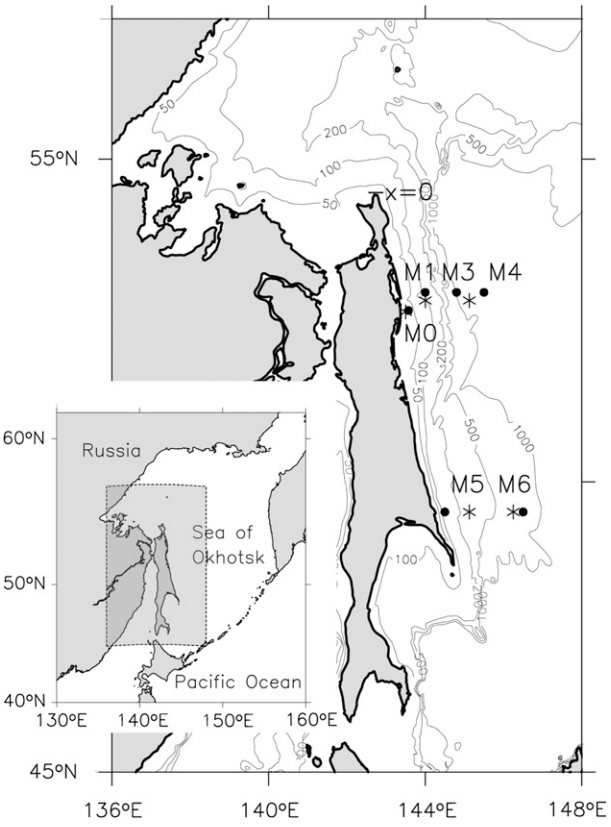

FIG. 8. Locations of the moorings and wind data used for the analysis. (bottom left) The entire region of the Sea of Okhotsk in which the rectangular region denotes the enlarged portion. Solid dots indicate the mooring sites and asterisks indicate the locations of the wind data. The location of $x = 0$ for the calculation of shelf waves is also shown.

along the north–south direction, the wind direction by which the sea ice is drifted parallel to the coast is toward the south-southeast, approximately 25° from the coast, which is somewhat different from the principal wind direction. Thus, in reality, open ocean (a coastal polynya) occasionally appears near the shore with the offshore wind and the convergence with internal stress would occur with the onshore wind. However, we discuss this issue later in the section 4 and assume the ideal case where sea ice is drifted by the wind exactly parallel to the coast.

The power spectral density of the wind is calculated for the component that drifts sea ice in the north–south direction. The spectral density of the wind decreases monotonically without any specific peak (not shown). We arbitrarily choose 0.1 cpd as a representative of low frequency and its wind speed is set to $|\hat{\mathbf{U}}_a| = 7$ m s^{-1} based on the band averaging over 0.007–0.2 cpd. Similarly, 0.35 cpd is chosen as a representative of high frequency and the speed is set to $|\hat{\mathbf{U}}_a| = 4$ m s^{-1} based on the band averaging over 0.2–0.5 cpd. The radar observation also showed that sea ice drift with about 0.1–0.2 cpd is

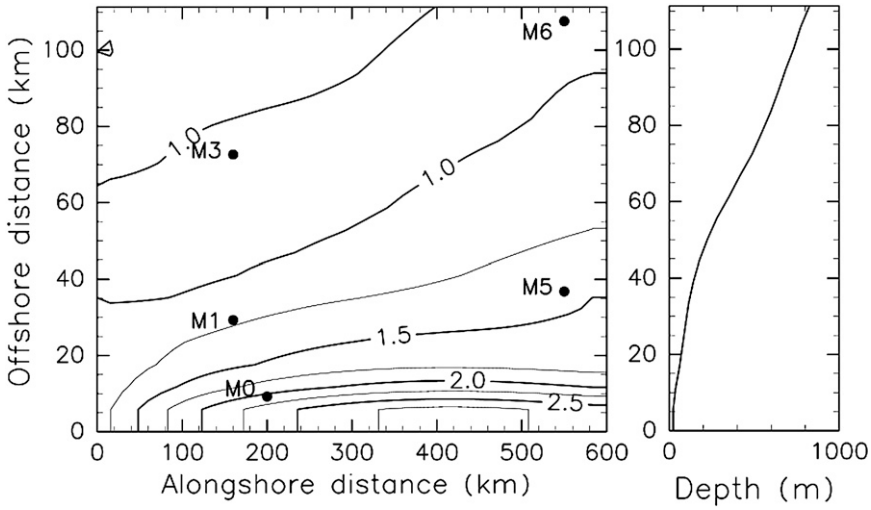

FIG. 9. (left) The spatial distribution of enhancement ratio γ calculated from modes 1–5 for (right) the depth profile off the coast of Sakhalin averaged over 49°–53°N, with $\hat{\mathbf{U}}_a = 7$ m s^{-1} and $\omega = 0.1$ cpd. The circles indicate the location of mooring stations M0–M6 in the averaged depth profile.

prominent off the Sakhalin coast (Shevchenko et al. 2004). The spatial distribution of γ for the case of 0.1 cpd is shown in Fig. 9, with the averaged depth profile off the Sakhalin coast (right panel). The circles indicate mooring stations whose information is shown in Table 1. The γ is enhanced within ~30 km from the coast with the maximum value exceeding 2.5. The region with larger γ expands downstream in accordance with the development of the shelf waves. When compared with the exponential profile case (Fig. 5b), the spatial distribution of γ is not significantly different, but γ is larger near the coast. This is because the minimum depth of 40 m near the coast is larger than the reality because of the fitting procedure to the exponential profile, and thus the amplitude of the ocean currents by shelf waves is weakened. The result for the case of 0.35 cpd is qualitatively similar to that for the case of 0.1 cpd (Table 2).

2) OBSERVATIONAL DATA

In this subsection, we use sea ice drift and ocean current data from the acoustic Doppler current profilers (ADCPs) deployed off the Sakhalin coast to examine whether the enhancement of sea ice drift can be observed in the real ocean as the theory predicts. The observations were conducted from July 1998 to June 2000 and from December 2002 to June 2003. The mooring locations are indicated in Fig. 8 and their information is summarized in Table 1. Further details of the observations are described in Mizuta et al. (2003) and Fukamachi et al. (2009).

The 10-m wind data at every 6 h from the ECMWF reanalysis were used here. The closest grid points of the wind data from the mooring stations used for the data analysis are indicated by the asterisks in Fig. 8. Only, at M0, in situ wind data were used for the analysis. The missing parts of the time series data were linearly interpolated. To compare with the theory, we only focus on the alongshore (north–south) sea ice drift and wind speed in the direction 25° from the alongshore direction, which drifts the sea ice roughly parallel to the coast.

As an example, we show the time series of the daily averaged alongshore sea ice drift, 3.5% of wind speed in

TABLE 1. Summarized information of the moorings from which ocean current and sea ice velocity data are used to obtain the apparent and exact wind factors.

Station	Lat (°N)	Lon (°E)	Bottom depth (m)	Measurement depth (m)	Period for data analysis
M0	52.7	143.5	32	13	27 Dec 2002–30 Apr 2003
M1	53.0	144.0	100	20	1 Dec 1998–30 Apr 1999
M3	53.0	144.8	480	20	16 Jan–30 Apr 1999
M4	53.0	145.5	1720	21	23 Jan–30 Apr 2000
M5	49.5	144.5	130	21	13 Dec 1998–30 Apr 1999
M6	49.5	146.5	790	24	1 Feb 1998–30 Apr 1999

TABLE 2. The values of γ, the ratio of the apparent to exact wind factors, calculated from the observational data and theoretical solutions at mooring stations M0–M6. For the observation, the values of γ calculated from the daily averaged data for the entire frequency range and those calculated from the 6-hourly data for low- (0.03–0.2 cpd) and high- (0.2–0.5 cpd) frequency ranges are shown. For the theoretical solutions, the results for $\omega = 0.1$ cpd and $\omega = 0.35$ cpd are shown. The theoretical solution at M4 is not calculated because the depth of M4 is deeper than the maximum depth of the depth profile used.

Station	Alongshore distance (km)	Depth (m)	Observation			Theory	
			γ (entire frequency)	γ (low frequency)	γ (high frequency)	γ (0.1 cpd)	γ (0.35 cpd)
M0	200	32	1.7	1.5	1.8	2.1	1.8
M1	160	100	1.7	2.0	1.3	1.2	1.1
M3	160	480	1.1	1.1	1.0	1.0	1.0
M4	160	1720	1.0	1.0	1.0	—	—
M5	550	130	1.4	3.5	1.3	1.4	1.1
M6	550	790	1.0	1.1	1.0	1.0	1.0

the direction 25° from the alongshore direction, and alongshore ocean current at M1 (Fig. 10). When we focus on the strong wind events that started from 2 March and 1 April (see the arrows), sea ice drift was first enhanced in response to the wind. Subsequently, the ocean current was also induced in the same direction as that of the wind with a phase lag of 1–3 days, which suggests the excitation of CTWs. Finally, sea ice drift was further enhanced by this ocean current. This feature seems to be consistent with the analytical result of the relationship among the wind-driven sea ice velocity, ocean current, and total sea ice velocity (Fig. 3). Even the raw time series suggest that the enhancement of sea ice drift due to the interaction between sea ice and a coastal ocean occurs in reality. To evaluate this enhancement quantitatively, we calculate the enhancement ratio of sea ice drift at all mooring stations.

As in the case of section 2d, we set the alongshore sea ice drift as X and the wind in the direction of 25° from the alongshore direction as Y. Using a least squares method, the apparent wind factor for the alongshore sea ice drift is obtained. Furthermore, the exact wind factor for the alongshore sea ice drift is obtained by subtracting the alongshore ocean current from the alongshore sea ice drift and using a least squares method similarly. The values of γ obtained from the daily averaged data during the analysis period for entire frequency are listed in the fourth column of Table 2. In addition, frequency analyses are conducted. For the frequency analyses, we used wind, sea ice velocity, and ocean current data at every 6 h. We divide the signals into low- (0.03–0.2 cpd) and high- (0.2–0.5 cpd) frequency components using the FFT and calculate the apparent and exact wind factors for each frequency range (Table 2). For comparison, we also show the values of γ at M0–M6 with 0.1 and 0.35 cpd from the theoretical solution. We set the northern edge of Sakhalin at $x = 0$, although in reality shelf waves might be somewhat excited from the region $x \leq 0$. The locations of M0–M6 in Fig. 9 (left) are defined by the actual alongshore distance (x) and the across-shore distance (y), which is determined from the location of the actual depth (shown in Table 2) in the averaged profile (right). This is because it is considered that the ocean current by shelf waves and thus γ depend more on depth rather than the actual offshore location.

3) COMPARISON BETWEEN THE THEORY AND OBSERVATION

In the theoretical solution for the periodic wind forcing, the enhancement is prominent over the shelf and decreases offshore converging to $\gamma = 1$ (Fig. 9), and the enhancement becomes smaller with higher wind frequency (not shown). It is noted that M1–M4 and M5–M6 are located at the same latitudes, respectively. In the observational data (Table 2), the values of γ near the coast (M0, M1, and M5) are relatively large (1.4–1.7), whereas those at deeper locations (M3, M4, and M6) are close to unity. The observations also show that the values of γ in the low frequency are larger than those in the high frequency,

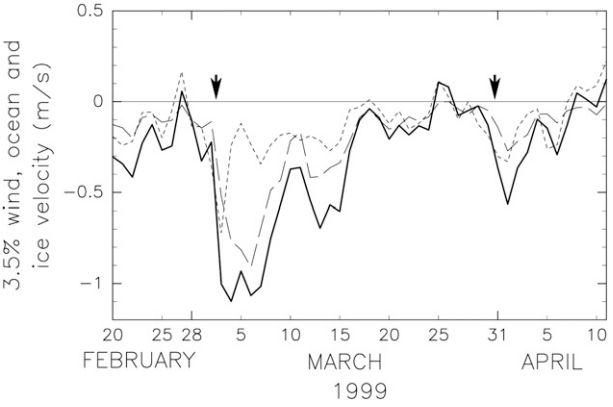

FIG. 10. Time series of 3.5% of wind speed in the direction 25° from the alongshore direction (dotted line), alongshore ocean current (dashed line), and alongshore sea ice velocity (thick solid line) at M1 from 20 Feb to 10 Apr 1999. The arrows indicate the strong wind events.

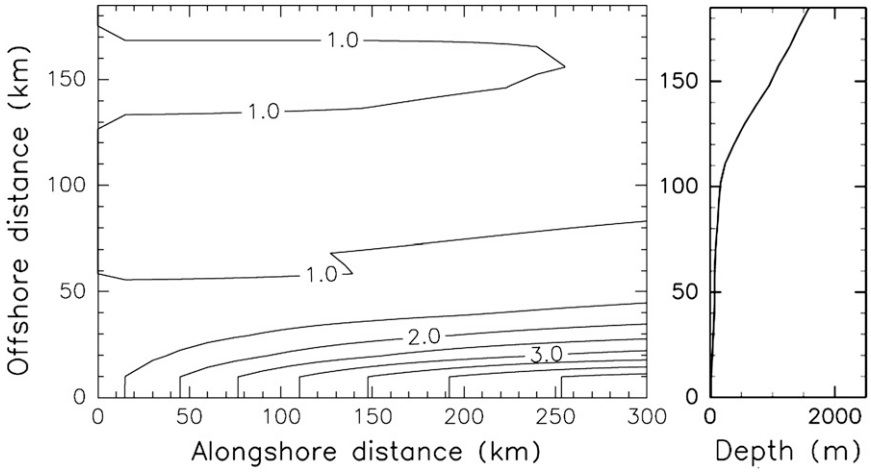

FIG. 11. (left) The spatial distribution of enhancement ratio γ calculated for (right) the depth profile off the Alaskan coast in the Chukchi Sea, averaged over 154°–159°W. The contour interval is 0.5.

except for the case at M0. In spite of the highly idealized setting, the values, spatial distribution and dependence of γ on frequency from the theory are mostly consistent with the observations.

However, there is an observational result inconsistent with the theory at M0: γ is smaller in the low frequency than that in the high frequency. If this inconsistency is real, the following scenario may explain the situation: Because M0 is located close to the coast, the sea ice drift field at M0 frequently changes between converging and diverging conditions over the winter. In the converging condition, it is likely to take some time for the internal stress of sea ice to become large enough to influence the motion of sea ice. For the case of the higher frequency, wind direction would change before the internal stress becomes significantly large. Meanwhile, for the case of the lower frequency, the internal stress would become significantly large and weaken the sea ice drift. As a result, the value of γ at M0 is larger in the high frequency than in the low frequency.

When γ_s is defined as the ratio of the averaged sea ice drift to the averaged sea ice drift minus the averaged ocean current underneath during the observational periods (Table 1) for the alongshore component, the observed γ_s is about 2–3 for all the locations of M0–M6. From the theoretical solution calculated under the realistic depth profile for the steady wind forcing, however, the enhancement is significant only near the coast (γ_s = 1.5 at M0) and is negligible at other locations (γ_s is close to unity), which is different from the observation. This is because the coastal current off the Sakhalin coast (East Sakhalin Current) has the component of the western boundary current by the wind stress curl as well as the arrested topographic wave induced by the alongshore wind stress (Simizu and Ohshima 2006). Thus, the observation and steady solution cannot be compared simply.

b. *Application to the regions off the Arctic and Antarctic coasts*

In this study, we have shown that sea ice drift is significantly enhanced in the coastal ocean where the free drift of sea ice roughly holds. Kimura and Wakatsuchi (2000) calculated the wind factor (actually the apparent wind factor) in the Northern Hemisphere using satellite-microwave data, and their results show that the wind factor is significantly large near the Alaskan coast in the Chukchi Sea, especially in December, January, and April (Kimura 2000). The similar analysis conducted in the Southern Ocean does not show any significant enhancement of the wind factor along the coast of the Antarctica (Kimura 2004). In this section, we apply our theory to these two regions.

The right panels of Figs. 11 and 12 show the depth profiles off the Alaskan coast in the Chukchi Sea averaged over 154°–159°W and off the coast of the East Antarctica averaged from 0° to 160°E, respectively. To compare the differences of the enhancement of sea ice drift as a result of the interaction between sea ice and a coastal ocean purely due to topographic features, the forcings and parameters are assumed to be the same in these two cases. We assume $C_a = C_w = 2.0 \times 10^{-3}$, as in section 2. In the Chukchi Sea, $C_a = 1.6 \times 10^{-3}$ and $C_w = 5.0 \times 10^{-3}$ were observed (Banke et al. 1980; McPhee 1982), and thus the assumed value of C_w is smaller than the observed value. Although in the Southern Ocean, $C_a = 1.9 \times 10^{-3}$ and $C_w = 1.5 \times 10^{-3}$ were observed in the Weddell Sea (Martinson and Wamser 1990; Andreas

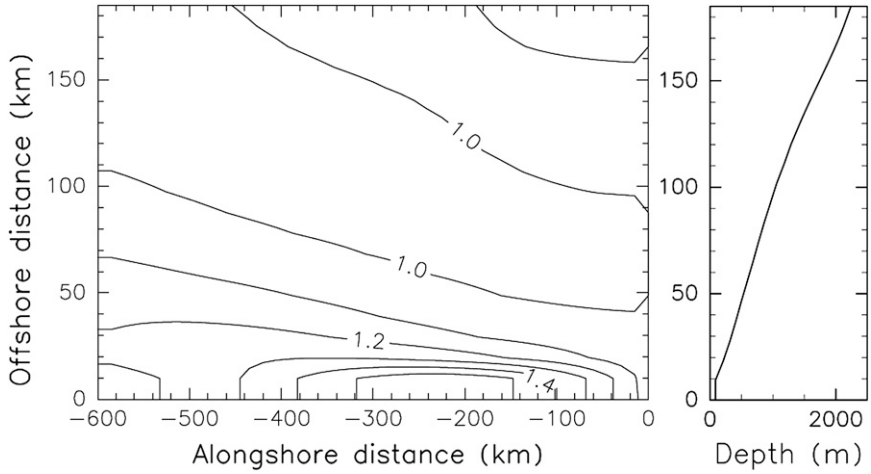

FIG. 12. (left) The spatial distribution of enhancement ratio γ calculated for (right) the depth profile averaged along the East Antarctic coast over 0°–160°E. The contour interval is 0.1.

and Claffey 1995), and thus the assumed values are similar to the observed ones. The winter-mean wind speed for the two regions ranges in 5–10 m s^{-1}. Here, we set $|\hat{\mathbf{U}}_a| = 10$ m s^{-1} and $\omega = 0.1$ cpd.

The spatial distributions of γ for the cases of the Chukchi Sea and off the East Antarctica are shown in the left panels of Figs. 11 and 12, respectively. The forcing and parameters are set to be the same as those used in sections 2 and 3, except that the spatially uniform wind is applied in the region of $x \leq 0$ for the case off the East Antarctica, because the propagation direction of the CTWs is opposite in the Southern Hemisphere. The enhancement is significant over the shelf within 50 km from the coast in the case of the Chukchi Sea, whereas the enhancement is fairly small in the case off the East Antarctica. This difference is mainly caused by the depth and the width of the shelves: a shallow broad shelf exists in the Chukchi Sea, whereas the depth increases rapidly from the coast off the East Antarctica. These results are consistent with the observed values of the apparent wind factors (Fig. 3 of Kimura and Wakatsuchi 2000; Fig. 4 of Kimura 2004). If we use $C_a = 1.6 \times 10^{-3}$ and $C_w = 5.0 \times 10^{-3}$, which are more realistic in the Chukchi Sea, γ becomes about 1.4 times larger, suggesting that γ could be even larger in the Chukchi Sea.

4. Summary and discussion

Sea ice drift is governed by wind forcing and interaction between sea ice and ocean. The previous observational studies (Kimura and Wakatsuchi 2000; Kimura 2004) showed that the wind factor, the ratio of sea ice speed to wind speed, tends to be large in some coastal oceans. This fact motivated us to study the coupling mechanism between sea ice and a coastal ocean that enhances sea ice drift. A schematic diagram of the coupling mechanism proposed in this study is depicted in Fig. 13. The mechanism is summarized as follows: First, sea ice is drifted by wind in the direction slightly to the right (left) of the wind direction in the Northern (Southern) Hemisphere. The wind stress over the sea ice generates the Ekman transport, which excites CTWs in the coastal ocean through stretching or shrinking of the water column by the Ekman compensated flow. Then, the ocean currents are induced underneath sea ice by the CTWs with larger amplitude closer to the coast, generally in the same direction as that of the wind-forced drift, resulting in the enhancement of sea ice drift.

This study investigated the enhancement of sea ice drift in highly idealized settings. We consider the case where spatially uniform oscillating wind drifts sea ice completely covering the ocean parallel to the coast. When barotropic

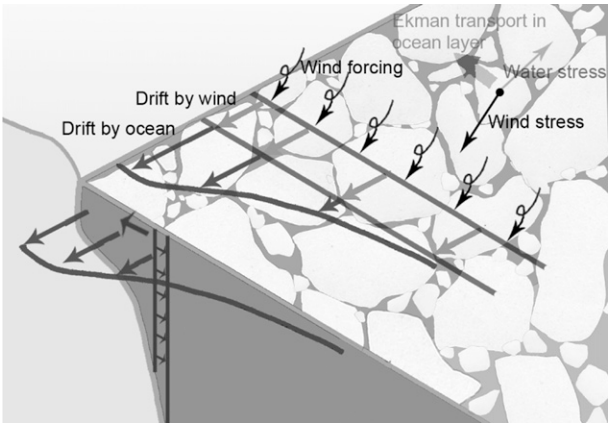

FIG. 13. A schematic diagram showing the enhancement mechanism of sea ice drift through the interaction between sea ice and a coastal ocean.

ocean response manifested by shelf waves is assumed, sea ice drifts driven by wind and ocean can be calculated analytically. Because the ocean current generated by shelf waves propagates along the coast, a phase difference exists between wind-driven and ocean-driven sea ice drifts. For the case of mode 1, which is generally the dominant mode, the phase difference remains small in the general alongshore scale of the coast and thus the sea ice drift is enhanced. To isolate the influence of the phase difference, we define γ as the ratio of the time-averaged value of sea ice drift driven both by wind and fluctuating ocean current to sea ice drift driven only by wind. The solutions of γ show that the larger enhancement of sea ice drift is prominent near the coast and that the region with larger γ expands downstream in accordance with the development of shelf waves.

Determining factors of the enhancement of sea ice drift is investigated using $\gamma - 1$, the ratio of the ocean current by the shelf waves to the wind-driven sea ice drift at the time when wind speed is the maximum. The ocean current by the shelf waves is proportional to a square of wind speed and air–ice drag coefficient [Eq. (18)]. On the other hand, sea ice drift driven by wind is proportional to wind speed and a square root of air–ice drag coefficient over ice–water drag coefficient (proportional to the Nansen number [Eq. (8)]. As a result, $\gamma - 1$ is proportional to wind speed and square roots of air–ice and ice–water drag coefficients [Eq. (17)]. When $\omega x/c_n \ll 1$, the ocean current and thus $\gamma - 1$ hardly depend on the wind frequency [Eq. (19)]; although $\omega x/c_n$ is not small, the ocean current and $\gamma - 1$ tend to be smaller with higher wind frequency [Eq. (18); Fig. 6].

From the analysis of the observations off the Sakhalin coast in the Sea of Okhotsk, it is shown that sea ice drift is enhanced up to 70% by ocean current near the coast. The frequency analyses show that the larger enhancement tends to occur at a lower frequency. These observed results are mostly consistent with the theoretical results (Table 2). We also apply our theory to the Alaskan coast in the Chukchi Sea and off the East Antarctica. The solutions show that the sea ice drift over the shelf is significantly enhanced in the case of the Chukchi Sea but not in the case off the East Antarctica (Figs. 11, 12), which is consistent with the analyses based on the satellite data (Kimura and Wakatsuchi 2000; Kimura 2004). The difference in the two oceans is mainly caused by the depth and the width of the shelves, which determine the strength of ocean current by shelf waves.

In this study, we model the dynamical interaction between sea ice and a coastal ocean in a highly simplified setting. In reality, sea ice concentration is not 100% all the time. When sea ice drifts toward the coast, the sea ice field becomes convergent and internal stress plays a significant role. On the other hand, when sea ice drifts off the coast, the sea ice field becomes divergent and a coastal polynya is formed. Comprehensive understanding of the dynamical interaction including such situations awaits future investigation. This study can be regarded as the first step to achieve this goal.

Acknowledgments. We thank Genta Mizuta, Takenobu Toyota, and Masaaki Wakatsuchi for their useful comments and suggestions. Figures were produced by GFD DENNOU Library. Insightful comments from the two anonymous reviewers were very helpful for improvement of the manuscript. This work was supported by the fund from Grant in Aids for Scientific Research (20221001) of the Japanese Ministry of Education, Culture, Sports, Science and Technology.

REFERENCES

Andreas, E. L, and K. J. Claffey, 1995: Air-ice drag coefficients in the western Weddell Sea 1. Values deduced from profile measurements. *J. Geophys. Res.,* **100,** 4821–4831.

Banke, E. G., S. D. Smith, and R. J. Anderson, 1980: Drag coefficients at AIDJEX from sonic anemometer measurements. *Sea Ice Processes and Models,* R. S. Pritchard, Ed., University of Washington Press, 430–442.

Chapman, D. C., J. A. Barth, R. C. Beardsley, and R. G. Fairbank, 1986: On the continuity of mean flow between the Scotian Shelf and the Middle Atlantic Bight. *J. Phys. Oceanogr.,* **16,** 758–772.

Csanady, G. T., 1978: The arrested topographic wave. *J. Phys. Oceanogr.,* **8,** 47–62.

Emery, W. J., C. W. Fowler, and J. A. Maslanik, 1997: Satellite-derived maps of Arctic and Antarctic sea ice motion: 1988 to 1994. *Geophys. Res. Lett.,* **24,** 897–900.

Fissel, D. B., and C. L. Tang, 1991: Response of sea ice drift to wind forcing on the northeastern Newfoundland shelf. *J. Geophys. Res.,* **96,** 18 397–18 409.

Fujisaki, A., H. Yamaguchi, T. Toyota, A. Futatsudera, and M. Miyanaga, 2009: Measurements of air-ice drag coefficient over the ice-covered Sea of Okhotsk. *J. Oceanogr.,* **65,** 487–498.

Fukamachi, Y., and Coauthors, 2009: Direct observations of sea-ice thickness and brine rejection off Sakhalin in the Sea of Okhotsk. *Cont. Shelf Res.,* **29,** 1541–1548.

Gill, A. E., and E. H. Schumann, 1974: The generation of long shelf waves by the wind. *J. Phys. Oceanogr.,* **4,** 83–90.

Greenan, B. J. W., and S. J. Prinsenberg, 1998: Wind forcing of ice cover in the Labrador shelf marginal ice zone. *Atmos.–Ocean,* **36,** 71–93.

Häkkinen, S., and D. J. Cavalieri, 2005: Sea ice drift and its relationship to altimetry-derived ocean currents in the Labrador Sea. *Geophys. Res. Lett.,* **32,** L11609, doi:10.1029/2005GL022682.

Heil, P., and I. Allison, 1999: The pattern and variability of Antarctic sea-ice drift in the Indian Ocean and western Pacific sectors. *J. Geophys. Res.,* **104,** 15 789–15 802.

Joffre, S. M., 1982: Momentum and heat transfers in the surface layer over a frozen sea. *Bound.-Layer Meteor.,* **24,** 211–229.

Kimura, N., 2000: A mechanism for the variation of sea-ice extent in the Northern Hemisphere. Ph.D. thesis, Hokkaido University, 72 pp.

——, 2004: Sea ice motion in response to surface wind and ocean current in the Southern Ocean. *J. Meteor. Soc. Japan,* **82,** 1223–1231.

——, and M. Wakatsuchi, 2000: Relationship between sea-ice motion and geostrophic wind in the Northern Hemisphere. *Geophys. Res. Lett.,* **27,** 3735–3738.

Leppäranta, M., 1998: The dynamics of sea ice. *Physics of Ice-Covered Seas,* M. Leppäranta, Ed., University of Helsinki Press, 305–342.

——, 2005: *The Drift of Sea Ice*. Springer, 266 pp.

Martinson, D. G., and C. Wamser, 1990: Ice drift and momentum exchange in the winter Antarctic pack ice. *J. Geophys. Res.,* **95,** 1741–1755.

McPhee, M. G., 1979: The effect of the oceanic boundary layer on the mean drift of sea ice: Application of a simple model. *J. Phys. Oceanogr.,* **9,** 388–400.

——, 1981: An analytical similarity theory for the planetary boundary layer stabilized surface buoyancy. *Bound.-Layer Meteor.,* **21,** 325–339.

——, 1982: Sea ice drag laws and simple boundary layer concepts, including application to rapid melting. U.S. Army Cold Regions Research and Engineering Laboratory Rep. 82–84, 25 pp.

——, 2008: *Air-Ice-Ocean Interaction: Turbulent Ocean Boundary Layer Exchange Processes*. Springer, 215 pp.

Mizuta, G., Y. Fukamachi, K. I. Ohshima, and M. Wakatsuchi, 2003: Structure and seasonal variability of the East Sakhalin Current. *J. Phys. Oceanogr.,* **33,** 2430–2445.

——, K. I. Ohshima, Y. Fukamachi, and M. Wakatsuchi, 2005: The variability of the East Sakhalin Current induced by winds over the continental shelf and slope. *J. Mar. Res.,* **63,** 1017–1039.

Nansen, F., 1902: *The Oceanography of the North Polar Basin, The Norwegian North Polar Expedition 1893–1896*. Scientific Results, Vol. 3, Kristiania, 427 pp.

Ohshima, K. I., 2000: Effect of landfast sea ice on coastal currents driven by the wind. *J. Geophys. Res.,* **105,** 17 133–17 141.

Ono, J., K. I. Ohshima, G. Mizuta, Y. Fukamachi, and M. Wakatsuchi, 2006: Amplification of diurnal tides over Kashevarov Bank in the Sea of Okhotsk and its impact on water mixing and sea ice. *Deep-Sea Res. I,* **53,** 409–424.

Overland, J. E., and C. H. Pease, 1988: Modeling ice dynamics of coastal seas. *J. Geophys. Res.,* **93,** 15 619–15 637.

Pease, C. H., and S. A. Salo, 1987: Sea ice drift near Bering Strait during 1982. *J. Geophys. Res.,* **92,** 7107–7126.

——, ——, and J. E. Overland, 1983: Drag measurements for first-year sea ice over a shallow sea. *J. Geophys. Res.,* **88,** 2853–2862.

Rabinovich, A. B., G. V. Shevchenko, and R. E. Thomson, 2007: Sea ice and current response to the wind: A vector regressional analysis approach. *J. Atmos. Oceanic Technol.,* **24,** 1086–1101.

Shevchenko, G. V., A. B. Rabinovich, and R. E. Thomson, 2004: Sea-ice drift on the northeastern shelf of Sakhalin Island. *J. Phys. Oceanogr.,* **34,** 2470–2491.

Simizu, D., and K. I. Ohshima, 2006: A model simulation on the circulation in the Sea of Okhotsk and the East Sakhalin Current. *J. Geophys. Res.,* **111,** C05016, doi:10.1029/2005JC002980.

Smith, S. D., 1972: Wind stress and turbulence over a flat ice floe. *J. Geophys. Res.,* **77,** 3886–3901.

Thorndike, A. S., and R. Colony, 1982: Sea ice motion in response to geostrophic winds. *J. Geophys. Res.,* **87,** 5845–5852.

Zubov, N. N., 1945: *L'dy Arktiki (Arctic Ice)*. Izdatel'stv Glavsevnorputi, 491 pp.